Metallophysics and Advanced Technologies
Металофіз. новітні технол.
Metallofiz. Noveishie Tekhnol.
2022, vol. 44, No. 10, pp. 1361–1375
https://doi.org/10.15407/mfint.44.10.1361
Reprints available directly from the publisher

PACS numbers: 61.72.-y, 81.05.Bx, 81.05.Mh, 81.20.Ev, 81.40.-z, 81.70.-q

Titanium-Based Layered Armour Elements Manufactured with 3*D*-Printing Approach

P. E. Markovsky, O. M. Ivasishin, D. G. Savvakin, O. O. Stasiuk, V. I. Bondarchuk, D. V. Oryshych, D. V. Kovalchuk*, S. H. Sedov**, V. A. Golub**, and V. V. Buznytskyi**

G. V. Kurdyumov Institute for Metal Physics N.A.S. of Ukraine,
36 Academician Vernadsky Blvd.,
UA-03142 Kyiv, Ukraine
**JSC 'NVO Chervona Hvylia'*
28 Dubrovytska Str.,
UA-04114 Kyiv, Ukraine
***The National Defence University of Ukraine Named After Ivan Chernyakhovskyi,*
28 Povitroflotskyi Ave.,
UA-03049 Kyiv, Ukraine

Triple layer titanium-based plate consisted of Ti–6Al–4V and CP–Ti layers 3*D*-printed on T110 substrate was tested for antiballistic protection. Microstructure after ballistic testing, hardness and three-point flexure characteristics of the layered material were studied and analysed. Interfaces between layers are important structure features contributing antiballistic protection characteristics. 3*D*-printed layers demonstrated sufficient bonding without porosity and other defects at interfaces, which resulted in promising antiballistic protection against high-energy B32 projectiles. Difference in microstructure, strength, hardness and ductile properties of individual layers resulted in noticeable variation of mechanical behaviour of layered materials depending on direction of applied force giving potential for further improvement of protecting characteristics.

Key words: titanium alloys, 3*D*-printing, multilayer materials, microstructure, armour, ballistic resistance, mechanical characteristics.

Corresponding author: Dmytro Savvakin
E-mail: savva@imp.kiev.ua

Citation: P. E. Markovsky, O. M. Ivasishin, D. G. Savvakin, O. O. Stasiuk, V. I. Bondarchuk, D. V. Oryshych, D. V. Kovalchuk, S. H. Sedov, V. A. Golub, and V. V. Buznytskyi, Titanium-Based Layered Armour Elements Manufacture with 3*D*-Printing Approach, *Metallofiz. Noveishie Tekhnol.*, **44**, No. 10: 1361–1375 (2022). DOI: 10.15407/mfint.44.10.1361

В роботі досліджено антибалістичні захисні характеристики трьохшарової плити, що складається з шарів стопу Ti–6Al–4V і технічно чистого титану, побудованих методою 3*D*-друку на підкладинці із стопу Т110. Після балістичних випробувань, досліджено і проаналізовано мікроструктуру, а також твердість та механічні характеристики даного шаруватого матеріялу при навантаженні методою 3-х точкового вигину. Поверхні між шарами є важливими структурними елементами, що вносять вклад в загальні захисні характеристики. 3*D*-друковані шари характеризуються достатньою силою зв'язку без пор та інших дефектів між ними, що забезпечує перспективні результати при захисті від бронебійних куль Б32. Різниця в мікроструктурі, міцности, твердости та пластичности індивідуальних шарів веде до зміни механічної поведінки шаруватих матеріялів в залежності від напрямку прикладеного навантаження, що дає потенціял для подальшого покращення захисних характеристик.

Ключові слова: титанові стопи, 3*D*-друк, багатошарові матеріяли, мікроструктура, броньовий захист, механічні характеристики.

(Received July 19, 2022; in final version, August 16, 2022)

1. INTRODUCTION

Titanium-based alloys and metal matrix composites are used in aerospace, medical, military and other applications owing to high strength to weight ratio and excellent corrosion resistance [1–3]. Among other applications, titanium-based materials are attractive for manufacturing of armour protecting elements for personnel and combat vehicles [3, 4], but relatively high cost of titanium makes this material less competitive compared to armour steels.

Despite attractive set of mechanical characteristics, conventional uniform titanium alloys like other uniform metallic materials possess limited combination of strength and ductile properties. For this reason, conventional titanium alloys sometimes do not ensure confident protection against ballistic impact and penetration of projectiles. Enhanced set of mechanical characteristics and better antiballistic protection can be achieved with creation of multi-layered structures owing to combination of various alloys and/or composites possessing noticeably different strength and ductile properties as entire article [5–10]. As an example, combination of high-strength hard composite or alloy layer with lower-strength alloy having increased fracture toughness and ductility allows to reach improved strength/ductility balance which is not achievable for individual uniform materials. Moreover, interfaces between layers in multi-layered structures can be important elements for scattering and dissipation of kinetic energy of projectiles [7].

3*D*-printing, also known as additive manufacturing (AM) [11–14]

technologies have a great potential for production of titanium-based and other metallic articles of complex shape, including multi-layered structures. Proper selection of 3*D*-printing parameters provides attractive mechanical characteristics of titanium-based articles for various applications and also promotes decreased manufacturing cost for near-net-shape products. The main research and development efforts were dedicated to AM of Ti–6Al–4V (wt.%) material as the most widely used titanium composition over the world [13–16]. At the same time, 3*D*-manufacturing approach has wide opportunities for variations in chemical composition and, hence, mechanical characteristics of entire articles and individual layers of their constituents.

The purpose of the present study was 3*D*-manufacturing of multi-layered structures consisted of titanium alloys possessing quite different strength and ductility levels; evaluation of their microstructure and antiballistic protecting potential.

2. MATERIALS AND EXPERIMENTAL PROCEDURE

Three-layer plate (Fig. 1) consisted of titanium alloys possessing different strength and ductile characteristics was manufactured and studied in present investigation. Industrially produced cast and wrought plate (10 mm thickness) of high-strength T110 alloy (Ti–

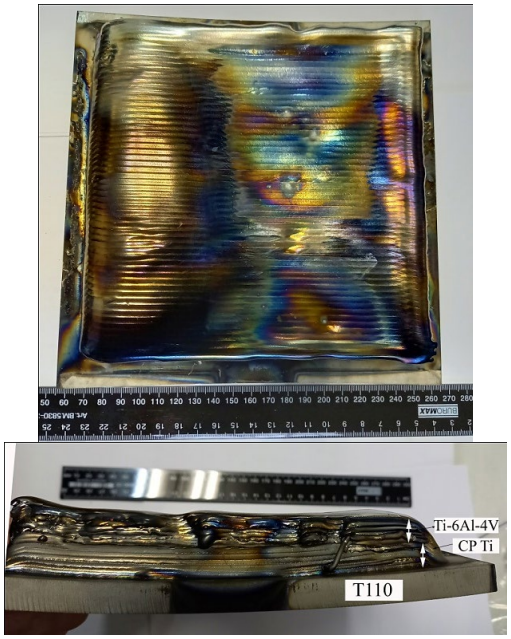

Fig. 1. Top and side view of manufactured 3-layer plate.

5.5Al–0.5Zr–4Nb–1.5V–1.5Mo–0.5Fe, wt.%) was used as substrate for 3*D*-printing of ductile low-strength CP–Ti layer and medium strength Ti–6Al–4V alloy layer. The main characteristics of obtained plate are listed in Table 1.

The CP–Ti and Ti–6Al–4V layers were deposed on T110 substrate with the xBeam 3*D* Metal Printing method [17–19], which used wires of corresponding compositions 3 mm in diameter and a profile electron beam as a hollow inverted cone to melt a wire which is fed coaxially with electron beam. Such electron beam configuration creates well controlled concentration of energy on the heating surface (in the range of 10^3 kW/cm^2) and provides desirable melting and cooling conditions, thus, giving a number of exceptional technological possibilities for manufacturing of high-quality articles [17–19]. CP–Ti layer 12 mm in thickness was built on T110 substrate with subsequent 3*D*-printing of top Ti–6Al–4V 12 mm layer (Fig. 1). Finally, manufactured 3-layer plate 190×190×34 mm was annealed in vacuum 10^{-3} Pa at 650°C for 4 h and cooled with furnace to reduce residual stresses in the material arose during intensive thermocycling (local rapid heating and cooling) upon 3*D*-processing.

Such structure of layered plate (materials with higher strength as outer layers and ductile intermediate layer) should promote effective stopping of projectile with possible its deformation and fracture by outer layers (Ti–6Al–4V or T110) while ductile CP–Ti layer in material depth is useful to prevent crack propagation and fracture of layered material as a whole.

Antiballistic protecting characteristics of manufactured plate were tested in certified laboratory at National University of Defence of Ukraine named after Ivan Chernyakhovsky using B-32 bullets (7.62 mm and 12.7 mm calibres). On testing, the projectiles acted on the 3-layers plate from both sides (Ti–6Al–4V and T110 layers) for comparison. Kinetic energy of each projectile was calculated basing on projectile velocity determined with laser measuring device for each shoot.

After ballistic testing, the plate was cut using spark erosion method to study the inner microstructure and fractured surfaces near projectile impact craters with Light Optical (LOM; Olympus IX 70 micro-

TABLE 1. Main characteristics of 3*D*-printed 3-layer plate.

No. of layer	Material	Thickness, mm	Method of production	Average hardness, HV
1	Ti–6Al–4V	12	3D-printed	377
2	CP–Ti	12	3D-printed	179
3 Base/substrate	T110	10	Conventional cast and wrought	365

scope, Japan) and Scanning Electron Microscopy (SEM; TESCAN VEGA 3, Czech Republic), equipped with EDS micro-analyser (Bruker QUANTAX, Germany). The hardness of individual layers was studied with Wolpert 432 SVD (Germany) tester and automatic tester Qness (Austria). Rectangular (55×10×10 mm) two-layered samples were cut with spark erosion at Ti–6Al–4V/CP–Ti as well as CP–Ti/T110 interfaces along the plate to evaluate 3 points flexure characteristics of interface areas between neighbouring layers using Instron 8802 machine.

3. RESULTS AND DISCUSSION

3.1. Characterization of Initial State of 3-Layer Material

The typical microstructures of the separate layers of 3*D*-printed material are shown in Fig. 2. Both 3*D*-printed layers (Fig. 2, *a*, *b*) demonstrated coarse-grained structures with clearly visible columnar-like β grains up to few mm length, and 0.2–1 mm width. The Ti–6Al–4V layer is characterized by fine lamellar α + β intragrain microstructure (Fig. 2, *a*), while in the CP–Ti layer a mixture of α crystals of lamellar and equiaxed morphologies up to 400 μm in size is observed (Fig. 2, *b*). Contrary, cast and wrought T110 substrate has relatively fine nearly equiaxed α + β microstructure, in which α-particles are elongated in rolling direction (Fig. 2, *c*). T110 and Ti–6Al–4V materials demonstrated relatively high average hardness (365 and 377 HV correspondingly, Table 1), such result is expected due to alloying strengthening and fine microstructure of wrought T110 plate as well as due to fine α + β intragrain microstructure of Ti–6Al–4V formed on rapid cooling during 3*D*-printing. CP–Ti layer has the lowest average hardness of 179 HV.

Used 3*D*-printing regimes ensured tight bonding and good adhesion between layers of different chemical composition without pores or other manufacturing defects at the interfaces. However, special attention should be paid to transition zones between the layers, which were formed upon melting of both materials during 3*D*-printing, because these areas undoubtedly have a special influence on the mechanical behaviour of a 3-layer structure. Fig. 2, *d* showed a typical example of microstructure of transition zone between 3*D*-printed CP–Ti layer and the T110 substrate. It is seen, that repeated heating and cooling during 3*D*-building of CP–Ti layer changed microstructure within upper part of cast and wrought T110 substrate from initially globular (Fig. 2, *c*) to fine lamellar inside heat affected zone (HAZ, Fig. 2, *d*). Alloying elements distribution within this transition zone (interface area) between CP–Ti and T110 layers within the same location is presented in Fig. 2, *e*. From comparison of Fig. 2, *e*, *d* it is clearly seen that the alloying elements, especially aluminium, quite deeply penetrated from the T110 substrate into the adjacent titanium layer.

It is expected that the presence of such a wide and smooth redistribution zone of alloying elements affects the mechanical characteristics. Indeed, the hardness values measured over the interface area (at an angle of 30° to the line crossing the interface in Fig. 2, *d* to obtain more accurate data) completely confirms the distribution of alloying elements (compare Fig. 2, *f*, *e*).

3.2. Results of Ballistic Testing

The general view of plate after ballistic testing is shown in Fig. 3. The plate was tested with 4 shoots (Table 2), including 3 shoots from Ti–

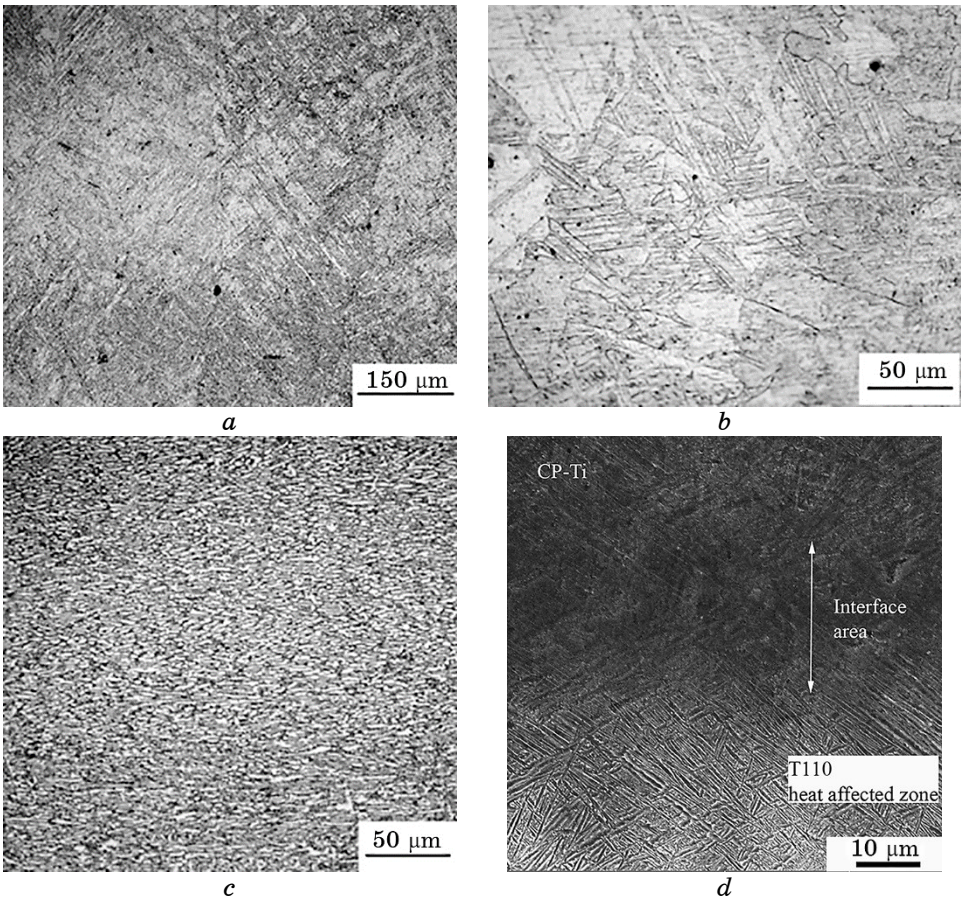

Fig. 2. Microstructures of 3*D*-printed Ti–6Al–4V (*a*) and CP–Ti layers (*b*), cast and wrought T110 substrate (*c*), interface between CP–Ti and T110 layers (*d*). Distribution of alloying elements (*e*) and *HV* microhardness (*f*) within transition zone shown in (*d*).

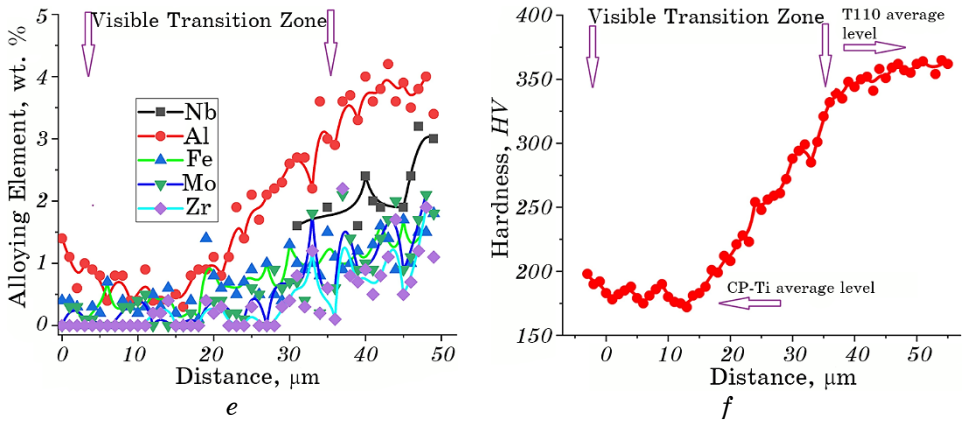

Continuation of Fig. 2.

6Al–4V alloy side and 1 shoot from opposite T110 alloy side. The type of projectiles, their kinetic energy and testing results are summarized in Table 2.

Projectiles Nos. 1 and 2 (both 12.7 mm calibre) slightly differs with their velocity and, hence, kinetic energies, which, however, led to quite different results. The projectile No. 1 was stopped within back T110 layer; this layer was fractured with delamination due to cracks formation near hard projectile core (Figs. 3, *b*, 4, *a*). It should be noted that this delamination occurred behind the fusion zone of CP–Ti and T110 layers and around or immediately behind of HAZ in T110 (see Fig. 2, *d*), in which there was a significant change in hardness (Fig. 2,

TABLE 2. Characteristics of used projectiles and results of shooting tests.

No. and side of shoot	Projectile/Bullet	Speed, m/s	Kinetic energy, J	Penetration depth, mm	Specific energy (kinetic energy/S), MJ/m^2
1. Ti–6Al–4V side	B32, 12.7 mm	820	16240	Pierced, but stopped in back T110 layer (34 mm)	131.34
2. Ti–6Al–4V side	B32, 12.7 mm	835	16838	Pierced	132.92
3. Ti–6Al–4V side	B32, 7.62 mm	835	3626	Not pierced, 21 mm	79.51
4. T110 side	B32, 7.62 mm	812	3429	Not pierced, 22 mm	75.19

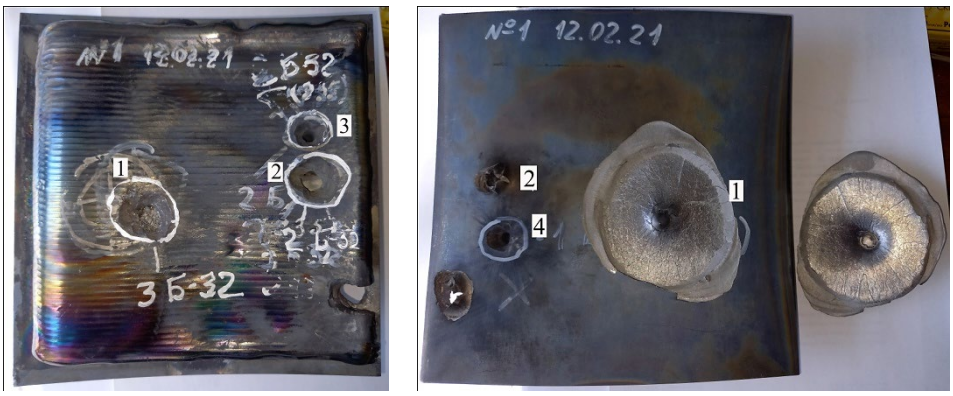

a *b*

Fig. 3. General view of plate after ballistic tests: Ti–6Al–4V alloy side (*a*), T110 alloy side showing delaminated fractured area near projectile No. 1 cavity (*b*).

f). The projectile No. 2 pierced entire plate with similar crack formation within T110 layer immediately behind HAZ (Fig. 4, *b*). Taking into account presented in Table 2 data, it is possible to conclude that difference in the kinetic energy of 598 J (*i.e.*, less than 4%) between bullets No. 1 and No. 2 is critical to overcome ballistic resistance of tested 3-layer plate.

Projectile No. 3 having lower 7.62 mm calibre, markedly lower kinetic energy and specific energy (kinetic energy of projectile divided by cross-section area of the crater, Table 2) pierced front Ti–6Al–4V layer and was stopped within next CP–Ti layer, the depth of impact area crater was 21 mm (Fig. 4, *c*). Shooting with opposite T110 side (projectile No. 4, 7.62 mm calibre) also resulted in projectile stopping within intermediate CP–Ti layer with similar penetration depth of 22 mm (Fig. 4, *d*). Despite the kinetic energy of projectile No. 3 exceeds the kinetic energy of projectile No. 4 by 197 J (or about 6%), the penetration depth of projectile No. 4 is greater by 1 mm (or 4.7%). From this result it is quite difficult to conclude how much the Ti–6Al–4V and T110 layers differ in their antiballistic properties, since they differ somewhat both in thickness and in the type of their microstructure. It can only be noted that due to the formation of some laminated structure in the T110 layer during rolling, transverse cracking occurred during the passage of a hardened steel core (see Fig. 4, *b*, *d*), which, as known, additionally absorbs the energy of shock waves [7].

3.3. Microstructure Investigations

Microstructure features of deformed layered plate near projectile impact craters are shown in Figs. 5–7. The rough and porous surfaces of

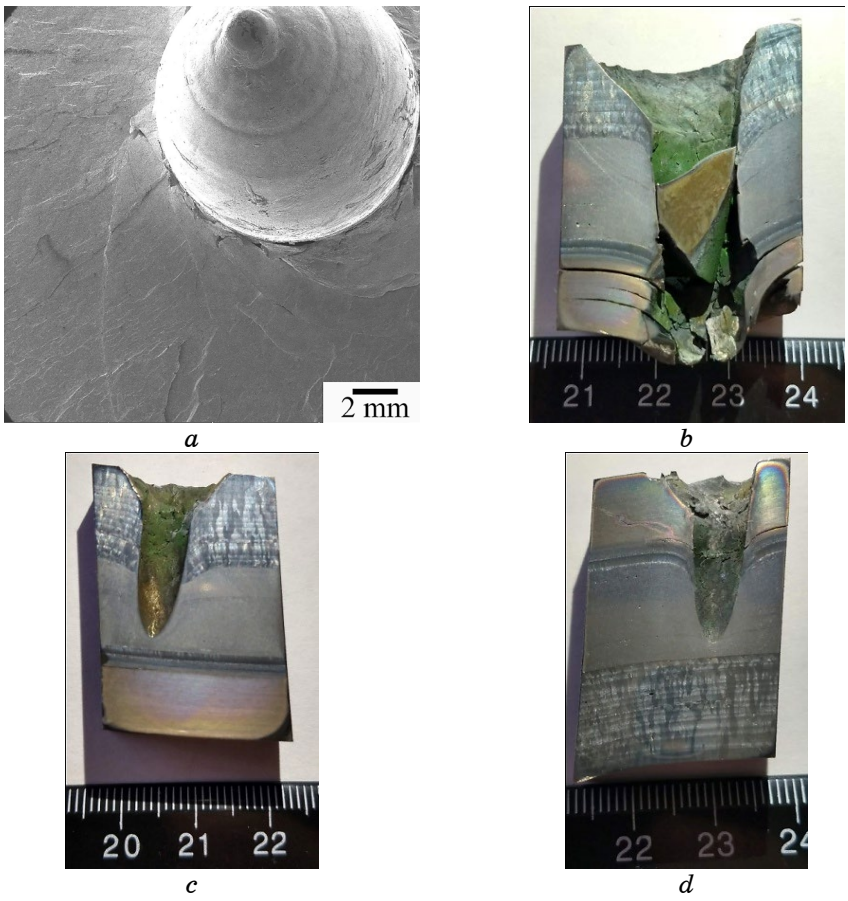

Fig. 4. Delaminated back T110 surface near projectile No. 1 impact area with a 12.7 mm bullet core stuck (*a*) and cross sections of the plate showing macrostructures near penetration channels of projectiles No. 2 (*b*), No. 3 (*c*), and No. 4 (*d*).

projectile craters (Fig. 5, *a*) are covered with lead of projectile shell molten on plate piercing. Independently on direction of projectile impact (either from Ti–6Al–4V or from T110 side) materials were severely deformed in the vicinity of craters with localized plastic flow and formation of adiabatic shear bands (ASB) in all affected layers. Cracking within individual layers as well as at the interfaces between adjacent layers was observed on high-speed deformation during ballistic impact (Fig. 5, *b*). Cracks nucleated at projectile crater and propagated in nearly perpendicular direction to crater axis (in parallel to layer interfaces), while ASB network propagated in various directions mainly along the projectile penetration craters (Fig. 5, *c*).

The main distortion with not uniform deformation was observed for front layer. For example, front Ti–6Al–4V layer was divided with ASB into blocks noticeably shifted from each other, but obvious traces of deformation were absent inside the blocks (Fig. 6, *a*). Interfaces between front and deeper layers were markedly deformed (Fig. 6, *a*) and cracked (Fig. 6, *b*). Formation of crack along the edge of T110 heat affected zone at the T110/CP–Ti interface (Fig. 6, *b*) can be explained with localization of residual stresses arose during 3*D*-processing and their partial preservation after annealing. Also, noticeable difference in mechanical characteristics between hardened finest lamellar $\alpha + \beta$ structure of T110 HAZ and neighbouring layers (soft ductile single phase α CP–Ti from one side and relatively ductile initial equiaxed $\alpha + \beta$ T110 structure from another side) can promote cracking in the vi-

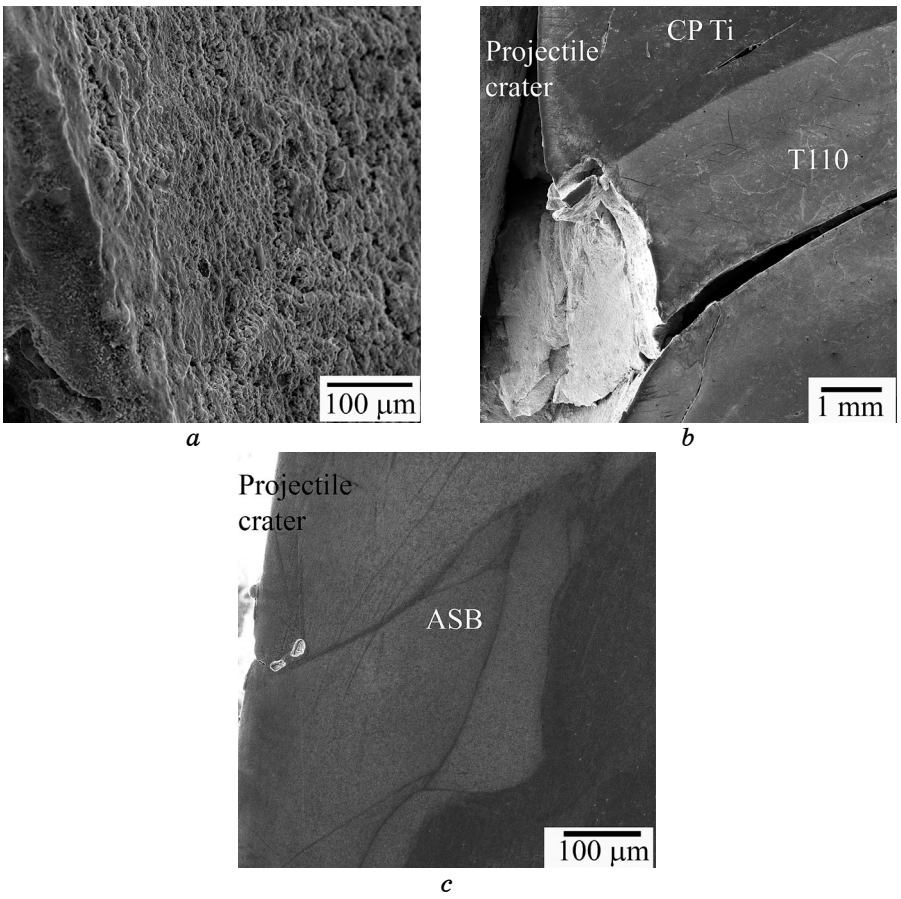

Fig. 5. Typical view of projectile crater (shoot No. 2) surface covered with lead (*a*) and general view of deformed layers near projectile crater (*b*) showing main directions of cracks propagation and adiabatic shear bands (*c*). Projectile impact direction is up to down.

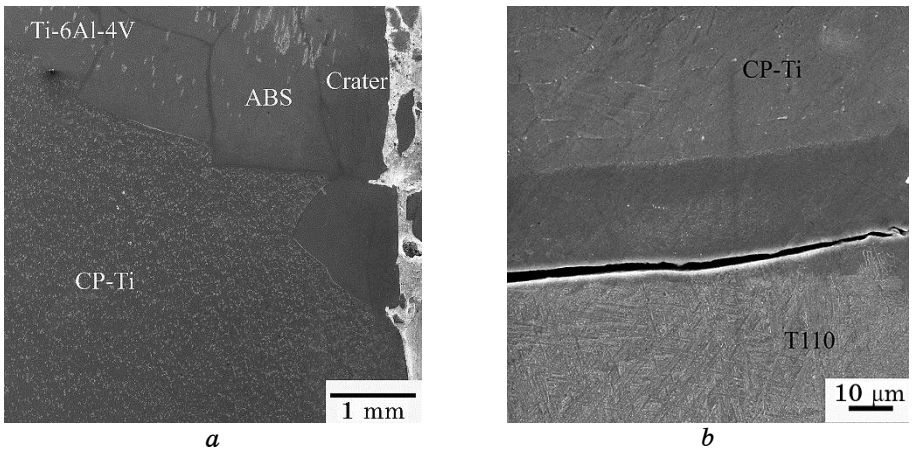

Fig. 6. Deformed interface between front Ti–6Al–4V and CP–Ti layers (*a*) and crack between front T110 and CP–Ti layers (*b*). Shoot No. 2.

cinity of HAZ during propagation and reflection of elastic stress waves at the interfaces.

High kinetic energy of projectiles Nos. 1–2 (Table 2) is a reason of entire plate piercing with fracture (Fig. 4, *a*) and delamination of back T110 layer. The fracture of T110 plate has mainly brittle mode (Fig. 7, *a*) with relatively low amount of ductile dimples. When T110 is a front layer (projectile No. 4, Table 2), well-developed ASB network and nucleation of cracks within severely deformed ASB areas was observed (Fig. 7, *b*) for this material. Interphase boundaries between α and β phase constituents were determined as weak locations responsible for crack initiation and propagation (Fig. 7, *c*). It should be noted, cracks are localized mainly within cast and wrought T110 layer (Fig. 4) while 3*D*-printed layers demonstrated much lower tendency for cracking. This fact suggests high potential of used 3*D*-manufacturing technology.

3.4. Points Flexure Test Results

Three points quasi-static flexure tests were performed for two-layered samples cut out from the 3*D*-printed plate in such a manner that will allow to evaluate the contribution of interfaces between different materials in antiballistic protection characteristics. The corresponding results are presented in Fig. 8. For both pairs of tested materials, side of external force loading is extremely important for mechanical behaviour, it is well known fact usually taken into consideration for construction of armour elements.

Loading from ductile CP–Ti layer resulted in higher strength char-

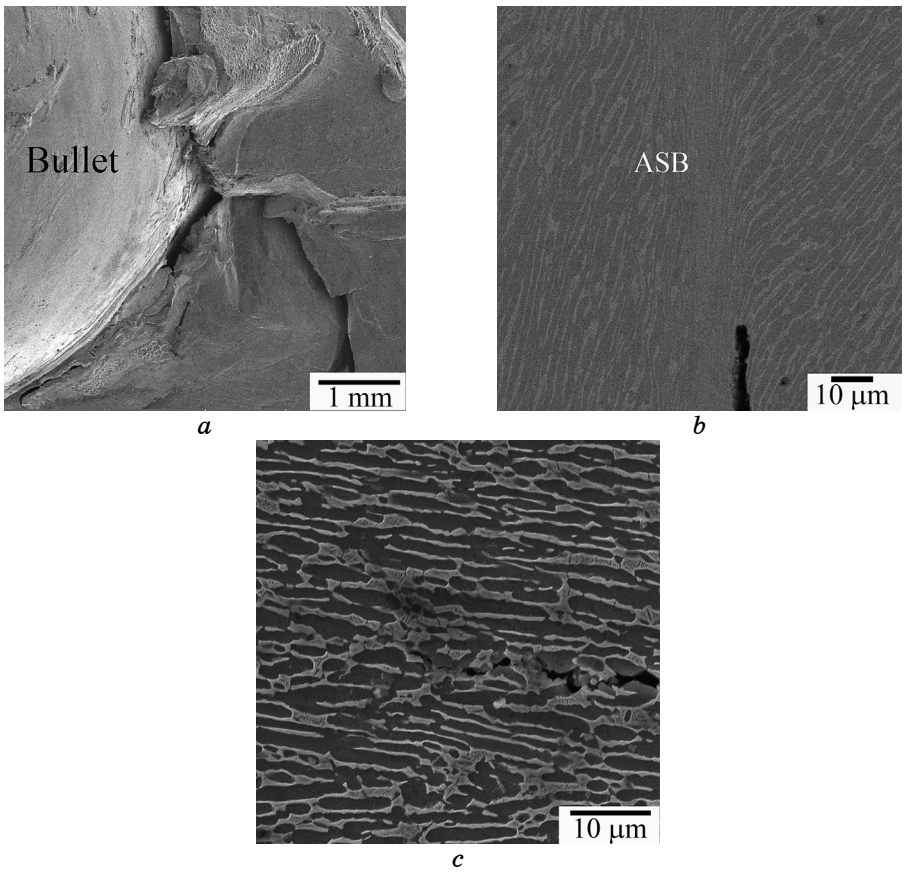

Fig. 7. Microstructure peculiarities of T110 layer: mainly brittle fractured back surface, projectile No. 1 (*a*); ASB with crack nucleated (*b*) and crack propagation between α and β phase constituents (*c*), projectile No. 4.

acteristics but fracture of back Ti–6Al–4V and T110 layers at relatively low strain values (Fig. 8, curves 1 and 3, correspondingly). If loading is performed from opposite side (*i.e.,* Ti–6Al–4V and T110 materials, curves 2 and 4), two-layer samples demonstrate reduced strength levels but considerably better strain characteristics with ductile failure mode due to high fracture toughness of back CP–Ti layer.

The 3-points flexure testing confirms generally known result about better protecting characteristics of layered materials in the case if high-strength material is used as front layer while quite ductile material is used as back layer. These data allow to make some additional comments on above results of ballistic tests.

The comparison of shoots No. 3 and No. 4 (both made with 7.62 mm projectiles at similar kinetic energies) shows that penetration depths

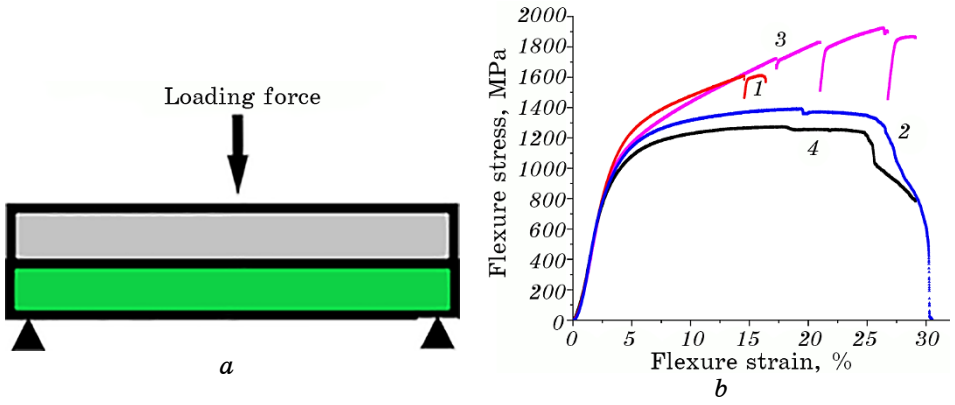

Fig. 8. Scheme of 3 points flexure test (*a*) and testing results for two-layer samples (b): Ti–6Al–4V/CP–Ti (1—loading from CP–Ti side and 2—from Ti–6Al–4V side); CP–Ti/T110 (3—loading from CP–Ti side and 4—from T110 side).

of projectiles are comparable independently on front side material for ballistic impact (either Ti–6Al–4V or T110 layers). Such result is expected because of hardness and thickness (Table 1) of both noted layers are comparable. Specific energies (kinetic energy/cross-section area of projectile crater ratio) of 7.62 mm projectiles (75–79 MJ/m^2, Table 2) are high enough to form penetration channel throughout Ti–6Al–4V and T110 layers of used thickness. Both outer materials did not able to deform hardened steel core of projectiles, but effective dissipation of their kinetic energies occurred on impact because of energy was spent for severe deformation of front layers and formation of craters. After that, projectiles with noticeably reduced residual energies were stopped within ductile CP–Ti layer.

The positive role of interfaces between layers, presumably, consists of not only reflecting of elastic stress waves [7]. Some part of projectile kinetic energy dissipated at the interfaces and spends to formation and propagation of cracks along the interfaces (as shown in Fig. 6). So, 7.62 mm projectiles (shoots Nos. 3, 4) with reduced residual energies can be easy stopped in next CP–Ti layer despite its lower strength and hardness. At the same time, higher bonding forces between the layers can be useful for better energy dissipation and, hence, better protecting characteristics of layered armour elements.

Because of 12.7 mm projectiles have significantly higher mass, kinetic energies and specific energies (Table 2, shoots Nos. 1, 2), both of them pierced all three layers with severe deformation of all materials (Fig. 4, *b*). The number of cracks formed near projectile impact crater and propagated along layers can be evidence of noticeable energy spent during projectile penetration. Delamination of back T110 layer (shoot

No. 1, Fig. 4, *a*) is also harmful for antiballistic protection. Increase in total material thickness and/or addition of once more ductile back layer can be recommended to improve protection against high-energy B-32 12.7 mm projectiles.

In general, experiments described in present study confirmed that layered titanium-based plate manufactured with 3*D*-printing approach can be effectively used as armour material for protection against 7.62 mm projectiles. For sustained protection against much more powerful 12.7 mm calibre bullets, materials layout in layered plates as well as thickness of individual layers and plates as a whole need further optimization

4. CONCLUSIONS

1. Titanium-based triple layer plate consisted of Ti–6Al–4V and CP–Ti layers 3*D*-printed on cast and wrought T110 substrate was tested for antiballistic protection against B32 projectiles of 7.62 mm and 12.7 mm calibres.
2. 3*D*-printed Ti–6Al–4V and CP–Ti layers possessed low propensity for cracking and fracture as well as sufficient bonding between layers without porosity and other defects at interfaces, while cast and wrought T110 substrate demonstrated higher tendency for cracking under high-energy ballistic impacts due to structure laminated on rolling and formation of hardened heat affected zone during 3*D*-processing.
3. Projectiles of 7.62 mm calibre were successfully stopped within inner CP–Ti layer independently on what side (either Ti–6Al–4V or T110) was selected as front layer. Markedly higher kinetic energy of 12.7 mm projectiles resulted in piercing of the entire triple plate of 34 mm thickness, but in the case of a little bit smaller kinetic energy of bullet its' core stuck in three-layer material.
4. Three points flexure testing confirmed noticeable variation of strength and ductile characteristics of layered materials depending on direction of applied force. Thus, proper combination of relatively strong and ductile materials as entire layered structure, including layout and thickness of individual materials is a promising way to achieve improved ballistic protecting characteristics.

ACKNOWLEDGMENT

This work was performed within the frames of the Agreement on scientific and technical cooperation between G. V. Kurdyumov Institute for Metal Physics, N.A.S. of Ukraine and the National Defence University of Ukraine named after Ivan Cherniakhovskyi. Part of microstructural

studies was performed under financial support of the project No. 3A-2022 from N.A.S. of Ukraine.

REFERENCES

1. G. Lutjering and J. C. Williams, *Titanium* (Berlin: Springer: 2007).
2. M. Peters, J. Kumpfert, C. H. Ward, and C. Leyens, *Adv. Engineering Mater.*, **5**, Iss. 6: 419 (2003).
3. T. L. Jones, K. Kondoh, T. Mimoto, N. Nakanishi, and J. Umeda, *Key Engineering Materials*, **551**: 118 (2013).
4. J. S. Montgomery and M. G. H. Wells, *JOM*, **4**: 29 (2001).
5. J. A. Zukas and D. R. Scheffler, *Int. J. Solids Structures*, **38**: 3321 (2001).
6. N. K. Gupta and V. Madlu, *Int. J. Impact Eng.*, **19**: 395 (1997).
7. J. K. Lee, *Analysis of Multi-Layered Materials under High Velocity Impact Using CTH* (Thesis of Disser. for Master Sci. in Aeronautical Engineering), 2685 (2008).
8. O. M. Ivasishin, P. E. Markovsky, D. G. Savvakin, O. O. Stasiuk, V. A. Golub, V. I. Mirnenko, S. H. Sedov, V. A. Kurban, and S. L. Antonyuk, *Usp. Fiz. Met.*, **20**, No. 2: 285 (2019).
9. P. E. Markovsky, D. G. Savvakin, S. V. Prikhodko, O. O. Stasyuk, S. H. Sedov, V. A. Golub, V. A. Kurban, and E. V. Stecenko, *Metallofiz. Noveishie Technol.*, **42**, No. 11: 1509 (2020).
10. P. E. Markovsky, D. G. Savvakin, O. O. Stasiuk, S. H. Sedov, V. A. Golub, D. V. Kovalchuk, and S. V. Prikhodko, *Metallofiz. Noveishie Technol.*, **43**, No. 12: 1573 (2021).
11. *Wohlers Report 2018. 3D Printing and Additive Manufacturing State of the Industry Annual Worldwide Progress Report*.
12. J. A. Harris, R. E. Winter, and G. J. McShane, *Int. J. Impact Eng.*, **104**: 177 (2017).
13. S. E. Alkhatib and T. B. Sercombe, *Mater. Design*, **217**: 110664 (2022).
14. Sh. Liu and Y. C. Shin, *Mater. Design*, **164**: 107552 (2019).
15. Donghong Ding, Bintao Wu, Zengxi Pan, Zhijun Qiu, and Huijun Li, *Mater. Manufacturing Processes*, **35**, Iss. 7: 845 (2020).
16. Jake Benzing, Nik Hrabe, Timothy Quinn, Ryan White, Ross Rentz, and Magnus Ahlfors, *Mater. Lett.*, **257**: 126690 (2019).
17. D. V. Kovalchuk, V. I. Melnik, I. V. Melnik, and B. A. Tugai, *Avtomatychne Zvaryuvannya* [Automatic Welding], No. 12: 26 (2017) (in Russian).
18. O. M. Ivasishin and D. V. Kovalchuk, *Additive Manufacturing for the Aerospace Industry. Chapter 12* (Eds. F. Froes and R. Boyer) (Elsevier: 2019).
19. D. Kovalchuk, V. Melnyk, I. Melnyk, D. Savvakin, O. Dekhtyar, O. Stasiuk, and P. Markovsky, *J. Mater. Eng. Perform.*, **30**(7): 5307 (2021).